arXiv:0808.0842v2 [hep-ph] 14 Jan 2009

Anomalous WWH couplings in $\gamma\gamma$ collision with initial beams and final state polarizations

Banu Şahin*

Department of Physics, University of Wisconsin, Madison, WI 53706, USA and

Department of Physics, Faculty of Sciences,

Ankara University, 06100 Tandogan, Ankara, Turkey

Abstract

The constraints on anomalous Higgs boson couplings are investigated through the process $\gamma\gamma \rightarrow W^+W^-H$. Considering the longitudinal and transverse polarization states of the final W^+ and W^- bosons and incoming beam polarizations, we find 95% confidence level limits on the anomalous coupling parameters Δa_W, b_W and β_W with an integrated luminosity of 500 fb^{-1} and $\sqrt{s}$=0.5, 1 TeV energies. We show that initial beam and final state polarizations lead to a significant improvement on the sensitivity limits of the anomalous coupling parameters b_W and β_W.

PACS numbers: 12.60.Fr, 13.66.Fg, 13.88.+e

---

[*] bsahin@wisc.edu; dilec@science.ankara.edu.tr

I. INTRODUCTION

The standard model (SM) of electroweak interactions based on the gauge group $SU(2)_L \times U(1)_Y$ has been verified to be successful in describing all the available precision experimental data. The recent measurements of gauge boson couplings at the CERN e^+e^- collider LEP and Fermilab Tevatron shed some light on the correctness of SM predictions for gauge boson interactions. On the other hand, the Higgs boson, which is a remnant of the spontaneous breaking of gauge symmetry, is the only undiscovered ingredient of the SM so far. The investigation of the electroweak symmetry breaking mechanism and the search for the Higgs boson constitute the prime targets of future colliders. Once the Higgs boson is found, its properties and interactions with other particles may be studied in detail with an e^+e^- collider and its $\gamma\gamma$, $e\gamma$ modes. However, the Higgs boson has not been discovered yet, there are experimental bounds for its mass. A lower bound on the Higgs mass is provided by direct searches at the LEP collider, $m_H > 114.4$ GeV [1]. Moreover, electroweak precision measurements provide an upper bound on its mass, $m_H < 186$ GeV [2].

In the literature there has been a great amount of work on Higgs interactions with gauge bosons. Higgs production modes proceed via its coupling with a pair of gauge bosons at a linear collider and deviations from their SM values are probed via such production processes. Anomalous WWH couplings have been investigated for the process $e^+e^- \to f\bar{f}H$ [3, 4, 5, 6], $e^+e^- \to W^+W^-\gamma$ [7], $e^-\gamma \to \nu_e W^- H$ [8] and $\gamma\gamma \to WWWW$ [9]. Anomalous gauge couplings of Higgs bosons have been analyzed at the LHC through the weak boson scattering [10] and vector boson fusion [11] processes.

At an e^+e^- collision Higgs boson production processes most often include both WWH and ZZH couplings and it is difficult to dissociate WWH from ZZH [3]. In this work we analyzed anomalous WWH vertex via the process $\gamma\gamma \to W^+W^-H$. This process isolates the WWH vertex and gives us the opportunity to study the WWH vertex independent of the ZZH. Furthermore, with Higgs and W bosons being visible (in their decay modes), one is offered a large amount of kinematical variables in the construction of suitable observables. Clearly, $e^-\gamma \to \nu_e W^- H$ process also isolates the WWH vertex as discussed in Refs.[8]. It was shown that initial and final state polarizations lead to a significant improvement in the sensitivity limits of the anomalous coupling parameters b_W and β_W. However, we will show that the $\gamma\gamma \to W^+W^-H$ process at the $\gamma\gamma$ mode of a linear collider has a higher potential to probe anomalous WWH couplings than $e^- \gamma \to \nu_e W^- H$. We take into account initial beams and final W boson polarizations to improve the sensitivity limits.

Deviations from SM expectations in the Higgs sector can be parameterized in a model independent way by an effective Lagrangian. We employ the effective lagrangian approach described in Ref.[3, 4, 5, 8]. If we demand Lorentz invariance and gauge invariance, the most general coupling structure (retaining up to dimension six terms in the effective lagrangian) can be expressed as

$$\Gamma^V_{\mu\nu} = i\tilde{g_V}\left[a_V g_{\mu\nu} + \frac{b_V}{m_V^2}(k_{2\mu}k_{1\nu} - g_{\mu\nu}k_1.k_2) + \frac{\beta_V}{m_V^2}\epsilon_{\mu\nu\alpha\beta}k_1^\alpha k_2^\beta\right] \tag{1}$$

with

$$\begin{aligned} \tilde{g}_W &= g_W m_W, \quad \tilde{g}_Z = \frac{g_W m_W}{cos^2\theta_W} \\ g_W &= \frac{g_e}{sin\theta_W}, \quad g_e = \sqrt{4\pi\alpha} \end{aligned} \tag{2}$$

where k_1^μ and k_2^μ are the momenta of two W's (or Z's). We consider that all the momenta are outgoing from the vertex. In the context of the SM, at the tree level, couplings are given by $a_V = 1$, $b_V = 0$ and $\beta_V = 0$. In our calculations we reparametrize the coupling a_V as $a_V = \Delta a_V + 1$, therefore within the SM $\Delta a_V = 0$.

II. POLARIZED CROSS SECTIONS

Experiments at future linear e^+e^- colliders will be able to investigate in detail the interactions of gauge bosons, fermions and scalars. In particular, one of the prime targets is the study of the interactions of the Higgs boson, for which the $\gamma\gamma$ mode of the collider seems especially suitable [12, 13, 14].

The process $\gamma\gamma \to W^+W^-H$ takes part as a subprocess in the e^+e^- collision. Real gamma beams which enter the subprocess are obtained through Compton backscattering of laser light off an electron and a positron beam, where most of the photons are produced at the high energy region. The luminosities for $e\gamma$ and $\gamma\gamma$ collisions turn out to be of the same order as that for e^+e^- [15], so the cross sections for photoproduction processes with real photons are considerably larger than the virtual photon case. The spectrum of the backscattered photons is given by [15]

$$f_{\gamma/e}(y) = \frac{1}{g(\zeta)}[1 - y + \frac{1}{1-y} - \frac{4y}{\zeta(1-y)} + \frac{4y^2}{\zeta^2(1-y)^2} + \lambda_0\lambda_e r\zeta(1-2r)(2-y)] \tag{3}$$

where

$$\begin{aligned} g(\zeta) = &\quad g_1(\zeta) + \lambda_0\lambda_e g_2(\zeta) \\ g_1(\zeta) = &\quad (1 - \frac{4}{\zeta} - \frac{8}{\zeta^2})\ln(\zeta+1) + \frac{1}{2} + \frac{8}{\zeta} - \frac{1}{2(\zeta+1)^2} && (4) \\ g_2(\zeta) = &\quad (1 + \frac{2}{\zeta})\ln(\zeta+1) - \frac{5}{2} + \frac{1}{\zeta+1} - \frac{1}{2(\zeta+1)^2} && (5) \end{aligned}$$

Here $r = y/[\zeta(1-y)]$ and $\zeta = 4E_eE_0/M_e^2$. E_0 and λ_0 are the energy and the helicity of the initial laser photon and E_e and λ_e are the energy and the helicity of the initial electron beam before Compton backscattering. y is the fraction which represents the ratio between the scattered photon and initial electron energy for the backscattered photons moving along the initial electron direction. The maximum value of y reaches 0.83 when $\zeta = 4.8$ in which the backscattered photon energy is maximized without spoiling the luminosity. Backscattered photons are not in fixed helicity states and their helicities are given by a distribution:

$$\xi(E_\gamma, \lambda_0) = \frac{\lambda_0(1-2r)(1-y+1/(1-y)) + \lambda_e r\zeta[1+(1-y)(1-2r)^2]}{1-y+1/(1-y) - 4r(1-r) - \lambda_e\lambda_0 r\zeta(2r-1)(2-y)} \tag{6}$$

where E_γ is the energy of backscattered photons. The helicity-dependent differential cross section for the subprocess can be written as

$$\begin{aligned} d\hat{\sigma}(\lambda_0^{(1)}, \lambda_0^{(2)}; \lambda_{W^+}, \lambda_{W^-}) = &\frac{1}{4}(1 - \xi_1(E_\gamma^{(1)}, \lambda_0^{(1)}))(1 - \xi_2(E_\gamma^{(2)}, \lambda_0^{(2)}))d\hat{\sigma}(-, -; \lambda_{W^+}, \lambda_{W^-}) \\ &+\frac{1}{4}(1 - \xi_1(E_\gamma^{(1)}, \lambda_0^{(1)}))(1 + \xi_2(E_\gamma^{(2)}, \lambda_0^{(2)}))d\hat{\sigma}(-, +; \lambda_{W^+}, \lambda_{W^-}) \\ &+\frac{1}{4}(1 + \xi_1(E_\gamma^{(1)}, \lambda_0^{(1)}))(1 - \xi_2(E_\gamma^{(2)}, \lambda_0^{(2)}))d\hat{\sigma}(+, -; \lambda_{W^+}, \lambda_{W^-}) \\ &+\frac{1}{4}(1 + \xi_1(E_\gamma^{(1)}, \lambda_0^{(1)}))(1 + \xi_2(E_\gamma^{(2)}, \lambda_0^{(2)}))d\hat{\sigma}(+, +; \lambda_{W^+}, \lambda_{W^-}) \end{aligned} \tag{7}$$

Here $d\hat{\sigma}(\lambda_\gamma^{(1)}, \lambda_\gamma^{(2)}; \lambda_{W^+}, \lambda_{W^-})$ is the helicity-dependent differential cross section, $\lambda_\gamma^{(i)} = +, -$ and $\lambda_V = +, -, 0$ ($V = W^+$, W^-). Superscripts (1) and (2) represent the incoming gamma beams and $\xi_1(E_\gamma^{(1)}, \lambda_0^{(1)})$ and $\xi_2(E_\gamma^{(2)}, \lambda_0^{(2)})$ represent the corresponding helicity distributions. The integrated cross section over the backscattered photon spectrums is given through the formula

$$d\sigma(e^+e^- \to \gamma\gamma \to W^+W^-H) = \int_{z_{min}}^{z_{max}} dz\, 2z \int_{z^2/y_{max}}^{y_{max}} \frac{dy}{y} f_{\gamma/e}(y) f_{\gamma/e}(z^2/y)\, d\hat{\sigma}(\gamma\gamma \to W^+W^-H) \tag{8}$$

where, $d\hat{\sigma}(\gamma\gamma \to W^+W^-H)$ is the cross section of the subprocess and the center of mass energy of the e^+e^- system, $\sqrt{s}$, is related to the center of mass energy of the $\gamma\gamma$ system, $\sqrt{\hat{s}}$, by $\hat{s} = z^2 s$.

In our calculations we accept that initial electron beam polarizability is $|\lambda_e| = 0.8$. To see the influence of initial beam polarization, the energy distribution of backscattered photons $f_{\gamma/e}$ is plotted for $\lambda_e\lambda_0 = 0, -0.8$ and $+0.8$ in Fig.1. It can be seen from the figure that backscattered photon distribution is very low at high energies in $\lambda_e\lambda_0 = +0.8$. Therefore we will consider the case $\lambda_e\lambda_0 < 0$ in the cross section calculations. If we interchange backscattered photon helicities the cross section does not change due to the symmetry. Moreover $(\lambda_0^{(1)}, \lambda_e^{(1)}, \lambda_0^{(2)}, \lambda_e^{(2)}) = (+1, -0.8, +1, -0.8)$ and $(\lambda_0^{(1)}, \lambda_e^{(1)}, \lambda_0^{(2)}, \lambda_e^{(2)}) = (-1, +0.8, -1, +0.8)$ combinations give the same cross section. So we have two different combinations: $(\lambda_0^{(1)}, \lambda_e^{(1)}, \lambda_0^{(2)}, \lambda_e^{(2)}) = (+1, -0.8, +1, -0.8)$ and $(-1, +0.8, +1, -0.8)$.

The process $\gamma\gamma \to W^+W^-H$ is described by eight tree-level diagrams (Fig.2). Each of the diagrams contains an anomalous WWH vertex. Helicity amplitude techniques have been used to obtain polarized amplitudes and the phase space integrations have been performed by GRACE [16] which uses a Monte Carlo routine.

One can see from Figs.3-5 the influence of the initial state polarizations on the deviations of the total cross sections from their SM value at $\sqrt{s} = 1$TeV. In Fig.3 the initial state polarization configuration $(\lambda_0^{(1)}, \lambda_e^{(1)}, \lambda_0^{(2)}, \lambda_e^{(2)}) = (+1, -0.8, +1, -0.8)$ coincides with $(-1, +0.8, +1, -0.8)$, therefore we plot one of them. We see from Fig.4 and Fig.5 that cross section for $(\lambda_0^{(1)}, \lambda_e^{(1)}, \lambda_0^{(2)}, \lambda_e^{(2)}) = (+1, -0.8, +1, -0.8)$ is more sensitive to the anomalous coupling parameters b_W and β_W than $(-1, +0.8, +1, -0.8)$. In Figs.6-8 we plot the total cross section as a function of anomalous parameters for various final state polarizations. In these figures TR and LO stand for "transverse" and "longitudinal" respectively. We consider all possible polarization combinations for the final W^+ and W^- bosons. In Fig.6 cross sections are plotted as a function of the parameter Δa_W. It is clear from the figure that the unpolarized cross section drastically grows as the parameter Δa_W increases. On the other hand, this growth in the cross section is relatively small for polarized cases. Therefore from Fig.6 we see that polarized cross sections are insensitive to the parameter Δa_W.

It can be extracted from figures that the most sensitive polarization configurations are $(\lambda_{W^+}, \lambda_{W^-})$ =(LO,LO) and (TR,LO). For instance in Fig.7, SM and anomalous cross sections at $b_W = 0.12$ are $\sigma_{SM} = 3.12 \times 10^{-4}$pb and $\sigma(b_W = 0.12) = 7.73 \times 10^{-2}$pb respectively for the polarization configuration (LO,LO). For the (TR,LO) case they are $\sigma_{SM} = 1.39 \times 10^{-3}$pb and $\sigma(b_W = 0.12) = 6.16 \times 10^{-2}$pb. Therefore we see that cross sections at the polarization configuration (LO,LO) and (TR,LO) increase by factor of 248 and 44 as b_W increases from 0 to 0.12. But this increment is only a factor of 10 in the unpolarized case; $\sigma_{SM} = 2.5 \times 10^{-2}$pb and $\sigma(b_W = 0.12) = 2.5 \times 10^{-1}$pb. It can be seen from Fig.8 that cross sections have a symmetric behavior as a function of the anomalous parameter β_W. Longitudinal W boson polarizations improve the deviations from the SM at both positive and negative values of β_W.

III. ANGULAR CORRELATIONS FOR FINAL STATE FERMIONS

The angular distributions of W^+ and W^- decay products have clear correlations with the helicity states of these final state gauge bosons. Therefore, in principle, polarization states of final W^+ and W^- bosons can be determined by measuring the angular distributions of W^+ and W^- decay products. This kind of analysis was done in reference [17] for the process $e^+e^- \to W^+W^-$. We consider the differential cross section for the complete process,

$$\begin{aligned}
\gamma(k_1, \lambda_\gamma^{(1)}) + \gamma(k_2, \lambda_\gamma^{(2)}) \to \quad & W^-(q_1, \lambda_{W^-}) + W^+(q_2, \lambda_{W^+}) + H(q_3) \\
& W^-(q_1, \lambda_{W^-}) \to f_1(p_1, \sigma_1)\bar{f}_2(p_2, \sigma_2) \\
& W^+(q_2, \lambda_{W^+}) \to f_3(p_3, \sigma_3)\bar{f}_4(p_4, \sigma_4)
\end{aligned} \tag{9}$$

with massless fermions $f_1, \bar{f}_2, f_3, \bar{f}_4$. Here $\lambda_\gamma^{(1)}$ and $\lambda_\gamma^{(2)}$ are the incoming photon helicities, λ_{W^-} and λ_{W^+} are the outgoing W^- and W^+ helicities. σ_i represent the helicities of final fermions f_i or $\bar{f}_i$.

The full amplitude can be written as follows:

$$M(k_1,\lambda_\gamma^{(1)};k_2,\lambda_\gamma^{(2)};q_3;p_i,\sigma_i) = D_{W^-}(q_1^2)D_{W^+}(q_2^2)\sum_{\lambda_{W^-}}\sum_{\lambda_{W^+}} M_1(k_1,\lambda_\gamma^{(1)};k_2,\lambda_\gamma^{(2)};q_1,\lambda_{W^-};q_2,\lambda_{W^+};q_3)$$
$$\times M_2(q_1,\lambda_{W^-};p_1,\sigma_1;p_2,\sigma_2)\times M_3(q_2,\lambda_{W^+};p_3,\sigma_3;p_4,\sigma_4) \tag{10}$$

where $M_1(k_1,\lambda_\gamma^{(1)};k_2,\lambda_\gamma^{(2)};q_1,\lambda_{W^-};q_2,\lambda_{W^+};q_3)$ is the production amplitude for $\gamma\gamma \to W^+W^-H$ with on-shell W^- and W^+. $M_2(q_1,\lambda_{W^-};p_1,\sigma_1;p_2,\sigma_2)$ and $M_3(q_2,\lambda_{W^+};p_3,\sigma_3;p_4,\sigma_4)$ are the decay amplitudes of W^- and W^+ to fermions. $D_{W^-}(q_1^2)$ and $D_{W^+}(q_2^2)$ are the Breit-Wigner propagator factors for W^- and W^+ bosons.

In this work we consider the hadronic decay channel of final state bosons. Therefore $f_1,\bar{f}_2,f_3,\bar{f}_4$ are quarks. M_2 and M_3 decay amplitudes are expressed in the rest frame of W^- and W^+ respectively. In the W^- rest frame, we parametrize f_1 and $\bar{f}_2$ four-momenta as

$$\begin{aligned} p_1^\mu &= \frac{m_W}{2}(1, sin\theta cos\phi, sin\theta sin\phi, cos\theta) \\ p_2^\mu &= \frac{m_W}{2}(1, -sin\theta cos\phi, -sin\theta sin\phi, -cos\theta) \end{aligned} \tag{11}$$

and in the W^+ rest frame, we choose the antiparticle ($\bar{f}_4$) angles as $\bar{\theta}$ and $\bar{\phi}$,

$$\begin{aligned} p_3^\mu &= \frac{m_W}{2}(1, -sin\bar{\theta} cos\bar{\phi}, -sin\bar{\theta} sin\bar{\phi}, -cos\bar{\theta}) \\ p_4^\mu &= \frac{m_W}{2}(1, sin\bar{\theta} cos\bar{\phi}, sin\bar{\theta} sin\bar{\phi}, cos\bar{\theta}) \end{aligned} \tag{12}$$

In this convention the angles of the d-type quark are chosen as (θ,ϕ) in W^- decays and $(\bar{\theta},\bar{\phi})$ in W^+ decays. M_2 and M_3 decay amplitudes are given by

$$M_2 = g_e g_-^{Wf_1f_2} C m_W \delta_{\sigma_{1,-}}\delta_{\sigma_{2,+}} l_{\lambda_{W^-}} \tag{13}$$

$$M_3 = -g_e g_-^{Wf_3f_4} \bar{C} m_W \delta_{\sigma_{3,-}}\delta_{\sigma_{4,+}} \bar{l}_{\lambda_{W^+}} \tag{14}$$

where

$$(l_-, l_0, l_+) = (\frac{1}{\sqrt{2}}(1+cos\theta)e^{-i\phi}, -sin\theta, \frac{1}{\sqrt{2}}(1-cos\theta)e^{i\phi}) \tag{15}$$

$$(\bar{l}_-, \bar{l}_0, \bar{l}_+) = (\frac{1}{\sqrt{2}}(1+cos\bar{\theta})e^{i\bar{\phi}}, -sin\bar{\theta}, \frac{1}{\sqrt{2}}(1-cos\bar{\theta})e^{-i\bar{\phi}}) \qquad (16)$$

Here $g_-^{Wf_1f_2}$ and $g_-^{Wf_3f_4}$ are the standard V-A coupling for quarks ($g_-^{Wf_1f_2} = g_-^{Wf_3f_4} = U_{ij}/\sqrt{2}sin\theta_W$). C and $\bar{C}$ denote the effective color factors ($\sqrt{3}$) for hadronic decay processes of the W^- and W^+.

Polarization summed squared matrix elements are given by

$$\sum_{\lambda_\gamma^{(1)},\lambda_\gamma^{(2)},\sigma_i} |M(k_1,\lambda_\gamma^{(1)};k_2,\lambda_\gamma^{(2)};q_3;p_i,\sigma_i)|^2 = |D_{W^-}(q_1^2)|^2|D_{W^+}(q_2^2)|^2 P^{\lambda_{W^-}\lambda_{W^+}}_{\lambda'_{W^-}\lambda'_{W^+}} D^{\lambda_{W^-}}_{\lambda'_{W^-}} \bar{D}^{\lambda_{W^+}}_{\lambda'_{W^+}} \qquad (17)$$

In this equation summation over repeated indices $(\lambda_{W^-}, \lambda'_{W^-}, \lambda_{W^+}, \lambda'_{W^+}) = +,-,0$ is implied. $P^{\lambda_{W^-}\lambda_{W^+}}_{\lambda'_{W^-}\lambda'_{W^+}}$ is the production tensor and $D^{\lambda_{W^-}}_{\lambda'_{W^-}}$, $\bar{D}^{\lambda_{W^+}}_{\lambda'_{W^+}}$ are the decay tensors for W^- and W^+ boson respectively. They are defined by

$$\begin{aligned} P^{\lambda_{W^-}\lambda_{W^+}}_{\lambda'_{W^-}\lambda'_{W^+}} = & \sum_{\lambda_\gamma^{(1)},\lambda_\gamma^{(2)}} M_1(k_1,\lambda_\gamma^{(1)};k_2,\lambda_\gamma^{(2)};q_1,\lambda_{W^-};q_2,\lambda_{W^+};q_3) \\ & \times M_1^*(k_1,\lambda_\gamma^{(1)};k_2,\lambda_\gamma^{(2)};q_1,\lambda'_{W^-};q_2,\lambda'_{W^+};q_3) \qquad (18) \end{aligned}$$

$$D^{\lambda_{W^-}}_{\lambda'_{W^-}} = \sum_{\sigma_1,\sigma_2} M_2(q_1,\lambda_{W^-};p_1,\sigma_1;p_2,\sigma_2) M_2^*(q_1,\lambda'_{W^-};p_1,\sigma_1;p_2,\sigma_2) \qquad (19)$$

$$\bar{D}^{\lambda_{W^+}}_{\lambda'_{W^+}} = \sum_{\sigma_3,\sigma_4} M_3(q_2,\lambda_{W^+};p_3,\sigma_3;p_4,\sigma_4) M_3^*(q_2,\lambda'_{W^+};p_3,\sigma_3;p_4,\sigma_4) \qquad (20)$$

The differential cross section can be written in the following form:

$$\begin{aligned} d\sigma = & \frac{1}{2s}|M|^2 \frac{d^3p_1}{(2\pi)^3 2E_{p_1}} \frac{d^3p_2}{(2\pi)^3 2E_{p_2}} \frac{d^3p_3}{(2\pi)^3 2E_{p_3}} \frac{d^3p_4}{(2\pi)^3 2E_{p_4}} \frac{d^3q_3}{(2\pi)^3 2E_{q_3}} \\ & \times (2\pi)^4 \delta^4(k_1+k_2-p_1-p_2-p_3-p_4-q_3) \qquad (21) \end{aligned}$$

Using narrow width approximation it is straightforward to express the differential cross section as

$$\begin{aligned} d\sigma = & \frac{1}{2s}(2\pi)^4\delta^4(k_1+k_2-q_1-q_2-q_3) \frac{\pi^2}{2^6(2\pi)^6\Gamma_{W^-}\Gamma_{W^+}m_W^2} \\ & \times P^{\lambda_{W^-}\lambda_{W^+}}_{\lambda'_{W^-}\lambda'_{W^+}} D^{\lambda_{W^-}}_{\lambda'_{W^-}} \bar{D}^{\lambda_{W^+}}_{\lambda'_{W^+}} \frac{d^3q_1}{(2\pi)^3 2E_{q_1}} \frac{d^3q_2}{(2\pi)^3 2E_{q_2}} \frac{d^3q_3}{(2\pi)^3 2E_{q_3}} dcos\theta d\phi dcos\bar{\theta} d\bar{\phi} \qquad (22) \end{aligned}$$

After integration over azimuthal angles ϕ and $\bar{\phi}$ interference terms will vanish and only the diagonal terms $\lambda_{W^-} = \lambda'_{W^-}$ and $\lambda_{W^+} = \lambda'_{W^+}$ will survive. The differential cross section can be written as

$$d\sigma = d\sigma_1(\lambda_{W^-}, \lambda_{W^+}) d^{\lambda_{W^-}}_{\lambda_{W^-}} \bar{d}^{\lambda_{W^+}}_{\lambda_{W^+}} \frac{9}{16} B(W^- \to f_1\bar{f}_2) B(W^+ \to f_3\bar{f}_4) dcos\theta dcos\bar{\theta} \tag{23}$$

Here $d\sigma_1(\lambda_{W^-}, \lambda_{W^+})$ is the helicity- dependent production cross section, $B(W^- \to f_1\bar{f}_2)$ and $B(W^+ \to f_3\bar{f}_4)$ are the branching ratios of W bosons to quarks. $d^{\lambda_{W^-}}_{\lambda_{W^-}}$ and $\bar{d}^{\lambda_{W^+}}_{\lambda_{W^+}}$ are related to the diagonal elements of decay tensors (19-20) as

$$\begin{aligned} d^{\lambda_{W^-}}_{\lambda_{W^-}} &= l_{\lambda_{W^-}} l^*_{\lambda_{W^-}} \\ \bar{d}^{\lambda_{W^+}}_{\lambda_{W^+}} &= \bar{l}_{\lambda_{W^+}} \bar{l}^*_{\lambda_{W^+}} \end{aligned} \tag{24}$$

The production cross section has nine different polarization configurations and identification of all nine polarized cross sections is difficult because of the necessity of charge (flavor) identification of both the W^- and W^+ decay products. Experimentally, in view of the difficulty of flavor identification there is an ambiguity in reconstruction of the polar angles of decay products. This makes it very difficult to identify polarization states $\lambda_{W^+} = +1, -1$ and $\lambda_{W^-} = +1, -1$ separately. On the other hand, cross section for the transverse polarization state which is the sum of $\sigma(\lambda_W = +1)$ and $\sigma(\lambda_W = -1)$ can be determined without an ambiguity. This is also true for the longitudinal polarization case. Therefore it is reasonable to claim that longitudinal (LO) and transverse (TR) polarizations can be identified [17]. Thus we define the following cross sections:

$$d\sigma_1(TR,TR) = \sum_{\lambda_{W^-}=+,-} \sum_{\lambda_{W^+}=+,-} d\sigma_1(\lambda_{W^-},\lambda_{W^+}) \tag{25}$$

$$d\sigma_1(LO,LO) = d\sigma_1(0,0) \tag{26}$$

$$d\sigma_1(TR,LO) = \sum_{\lambda_{W^-}=+,-} d\sigma_1(\lambda_{W^-},0) \tag{27}$$

$$d\sigma_1(LO,TR) = \sum_{\lambda_{W^+}=+,-} d\sigma_1(0,\lambda_{W^+}) \tag{28}$$

$$d\sigma_1(TR,unpol) = d\sigma_1(TR,TR) + d\sigma_1(TR,LO) \tag{29}$$

$$d\sigma_1(LO,unpol) = d\sigma_1(LO,TR) + d\sigma_1(LO,LO) \tag{30}$$

$$d\sigma_1(unpol,TR) = d\sigma_1(TR,TR) + d\sigma_1(LO,TR) \tag{31}$$

$$d\sigma_1(unpol,LO) = d\sigma_1(TR,LO) + d\sigma_1(LO,LO) \tag{32}$$

For fixed W^- and W^+ helicities above cross sections can be obtained from a fit to polar angle distributions of the W^- and W^+ decay products in the W^- and W^+ rest frames. More specifically, for $\lambda_{W^-} = \pm 1, 0$ polarization states of final W^-, production cross sections $d\sigma_1(\pm, \lambda_{W^+})$ and $d\sigma_1(0, \lambda_{W^+})$ can be obtained from a fit to d_+^+, d_-^- and d_0^0 distributions in the W^- rest frame (eqn.(23)). Similarly production cross sections $d\sigma_1(\lambda_{W^-}, \pm)$ and $d\sigma_1(\lambda_{W^-}, 0)$ can be obtained from a fit to $\bar{d}_+^+$, $\bar{d}_-^-$ and $\bar{d}_0^0$ distributions in the W^+ rest frame. In Fig. 9 $d_{\lambda_{W^-}}^{\lambda_{W^-}}$ distribution is plotted for various polarization states of final W^- boson. As can be seen from the figure, longitudinal (LO) and transverse (TR) distributions are well separated from each other.

IV. SENSITIVITY TO ANOMALOUS COUPLINGS

We have obtained 95% C.L. limits on the anomalous coupling parameters Δa_W, b_W and β_W using a simple χ^2 analysis at $\sqrt{s} = 0.5$ and 1 TeV energies and an integrated luminosity $L_{int} = 500 fb^{-1}$ without systematic errors. All our numerical calculations are for a Higgs mass of 120 GeV, hence the dominant decay mode should be $H \to b\bar{b}$ with a branching ratio $B_H \approx 0.9$.

In the literature there have been several experimental studies for the measurement of W polarization [18]. Angular distribution of the W boson decay products has a clear correlation with the helicity states of it. Therefore it is reasonable to assume that W boson polarization can be measured. We consider the case in which W momentum is reconstructible. We take into account the $W \to q\bar{q}'$ decay channel with a branching ratio $B_W \approx 0.68$. The expected number of events are given by $N = E(B_W)^2 B_H L_{int}\sigma$, where E is the b-tagging efficiency and it is taken to be 0.7 as in Refs. [3, 8].

In Table I-II we show 95% C.L. sensitivity limits on the anomalous coupling parameters Δa_W, b_W and β_W for $\sqrt{s} = 1$ and 0.5 TeV energies. In the tables, LO, TR represent the longitudinal, transverse polarization states and TR+LO describes the unpolarized W^+ and W^- bosons, $(\lambda_0^{(1)}, \lambda_e^{(1)}, \lambda_0^{(2)}, \lambda_e^{(2)}) = (0, 0, 0, 0)$ stand for the unpolarized initial beams.

We see from Table I that polarization leads to a significant improvement on the upper bound of b_W. Polarized bounds are compared with unpolarized bounds which are given in the first line of the table. The initial state $(\lambda_0^{(1)}, \lambda_e^{(1)}, \lambda_0^{(2)}, \lambda_e^{(2)}) = (-1, +0.8, +1, -0.8)$ together with the final state $(\lambda_{W^+}, \lambda_{W^-})$ =(LO,LO) polarization configuration improves the upper bound of b_W by a factor of 7.8. Final state (TR,TR) polarization combined with initial state polarizations improves the lower bound of b_W by a factor of 1.3. $(+1, -0.8, +1, -0.8)$ initial state with (LO, LO) final state polarization configuration improves both upper and lower bounds of β_W by a factor of 2.8 at $\sqrt{s} = 1$ TeV. These improvement factors are smaller for $\sqrt{s} = 0.5$ TeV. In Table II, $(-1, +0.8, +1, -0.8)$ together with (LO,TR+LO) improves the upper bound of b_W by a factor of 2.3. However limits on Δa_W are improved slightly by the initial state polarizations.

As we have mentioned in the introduction, WWH couplings are isolated also by the process $e^-\gamma \to \nu_e W^- H$ [8]. Our limits on the upper bound of b_W are a factor from 6 to 8.7 better than the bounds obtained in $e^-\gamma \to \nu_e W^- H$ depending on energy. The lower bound of b_W is approximately 1.7 times better at $\sqrt{s} = 1$ TeV. On the other hand at $\sqrt{s} = 1$ TeV, our bounds on β_W are 1.8 times better than the bounds acquired in $e^-\gamma \to \nu_e W^- H$.

For further analysis one can consider the systematic errors. The expected sources of systematic errors may result from the uncertainty on the measurement of $\gamma\gamma$ luminosity, helicity of incoming photons after Compton backscattering and uncertainty on the photon spectra. Moreover, the systematic uncertainties on the measurement of angular distributions of the decay products of the W bosons can be considered. For more precise results, further analysis needs to be supplemented with a more detailed knowledge of the experimental conditions.

In conclusion, we have obtained a considerable improvement in the sensitivity bounds of the anomalous parameters b_W and β_W by taking into account incoming beam polarizations and the final state polarizations of the W bosons. The subprocess $\gamma\gamma \to W^+W^-H$ in the $\gamma\gamma$ mode of a linear collider isolates WWH couplings and provide sensitive limits. Thus $\gamma\gamma$ colliders are better equipped than e^+e^- and $e\gamma$ colliders to study these couplings.

Acknowledgments

The author acknowledges support through The Scientific and Technological Research Council of Turkey (TUBITAK) BIDEB-2219 grant.

[1] R. Barate *et al.*, Phys. Lett. B 565, 61 (2003).

[2] LEP Electroweak Working Group, http://lepewwg.web.cern.ch/LEPEWWG/.

[3] S. S. Biswal, D. Choudhury, R. M. Godbole, and R. K. Singh, Phys. Rev. D 73, 035001 (2006).

[4] M. C. Gonzalez-Garcia, Int.J.Mod.Phys. A14, 3121 (1999).

[5] V. Barger, T. Han, P. Langacker, B. McElrath and P. Zerwas, Phys. Rev. D67, 115001 (2003).

[6] S. Dutta, K. Hagiwara and Y. Matsumoto, arXiv:0808.0477 [hep-ph].

[7] M.C. Gonzalez-Garcia, S. M. Lietti and S. F. Novaes, Phys. Rev. D59, 075008 (1999).

[8] D. Choudhury and Mamta, Phys. Rev. D 74, 115019 (2006);
İ. Şahin, Phys. Rev. D 77, 115010 (2008).

[9] T. Han, Y-P. Kuang and B. Zhang, Phys. Rev. D 73, 055010 (2006).

[10] H.-J. He, Y.-P. Kuang, C.-P. Yuan and B. Zhang, Phys. Lett. B 554, 64 (2003);
B. Zhang, Y.-P. Kuang, H.-J. He and C.-P. Yuan, Phys. Rev. D 67, 114024 (2003).

[11] V. Hankele, G. Klämke, D. Zeppenfeld and T. Figy, Phys. Rev. D 74, 095001 (2006).

[12] O. J. P. Éboli, M. C. Gonzalez-Garcia and S. F. Novaes, Phys. Rev. D 50, 3546 (1994);
O. J. P. Éboli, M. C. Gonzalez-Garcia, F. Halzen and D. Zeppenfeld, Phys. Rev. D 48, 1430 (1993);
J. F. Gunion and H. E. Haber Phys. Rev. D 48, 5109 (1993).

[13] M. Baillargeon and F. Boudjema, Phys. Lett. B 317, 371 (1993).

[14] E. Boos, I. Ginzburg, K. Melnikov, T. Sack and S. Shichanin, Z. Phys. C 56, 487 (1992);
K. Cheung, Phys. Rev. D 47, 3750 (1993).

[15] I.F. Ginzburg et al., Nucl. Instrum. Methods 205, 47 (1983);
I.F. Ginzburg et al., Nucl. Instrum. Methods 219, 5 (1984).

[16] T. Kaneko in "New Computing Techniques in Physics Research", ed. D. Perret-Gallix, W. Wojcik (Paris: Edition du CNRS) 1990;
MINAMI-TATEYA group, "GRACE manual", KEK Report 92-19, 1993;
F. Yuasa *et al.*, Prog. Theor. Phys. Suppl. 138, 18 (2000).

[17] K. Hagiwara et al., Nucl. Phys. B 282, 253 (1987).

[18] G. Abbiendi et al. (OPAL Collaboration), Eur. Phys. J. C19, 229 (2001); Phys. Lett. B585, 223 (2004); P. Achard et al. (L3 Collaboration), Phys. Lett. B557, 147 (2003).

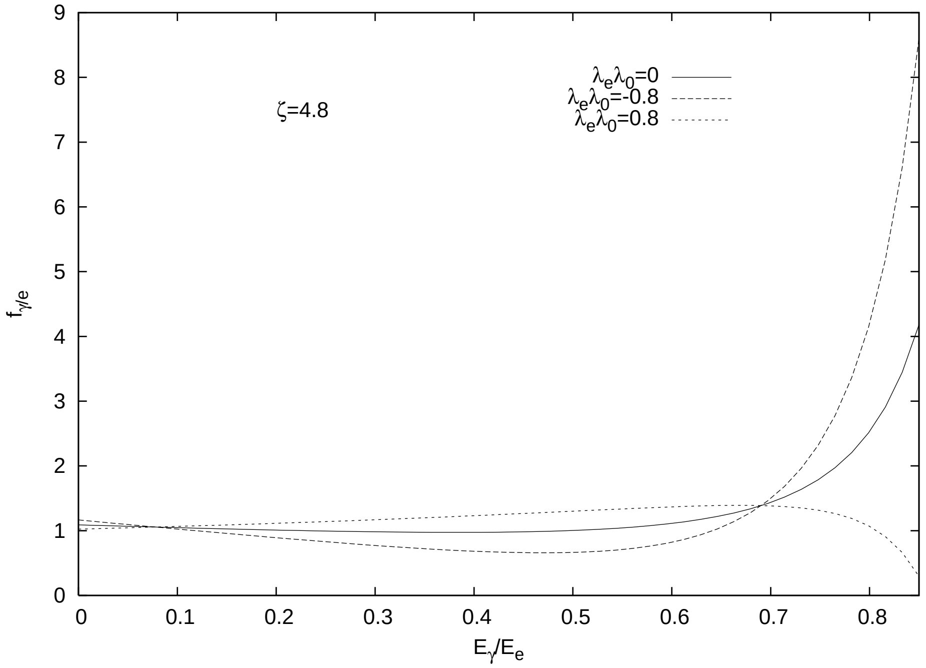

FIG. 1: Energy distribution of backscattered photons for $\lambda_e\lambda_0 = 0, -0.8, 0.8$.

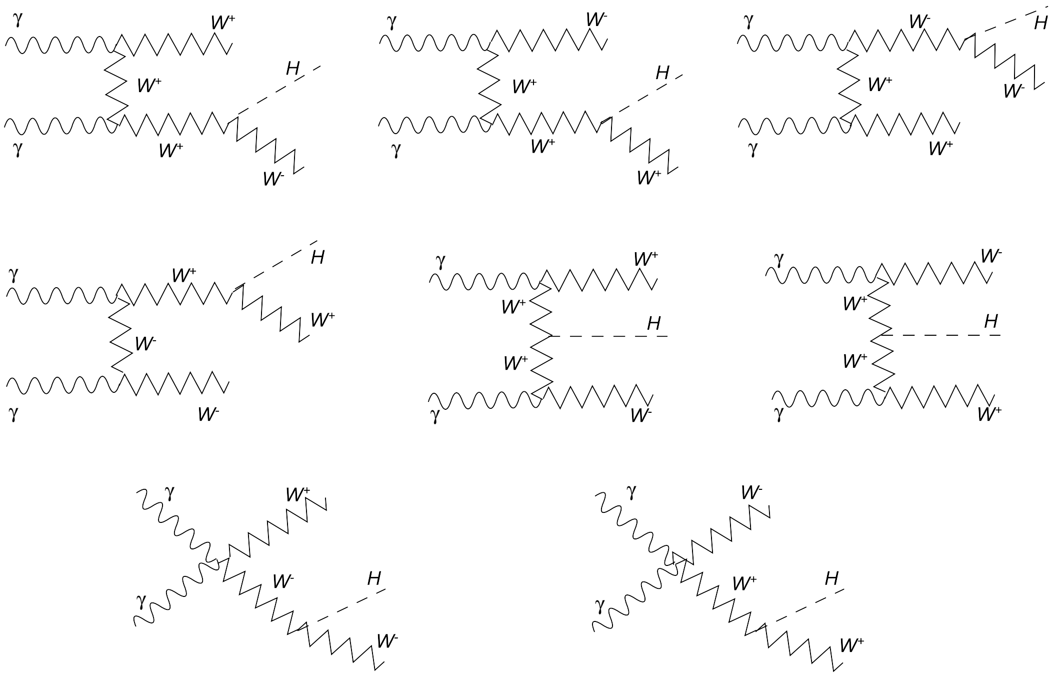

FIG. 2: Tree-level Feynman diagrams for $\gamma\gamma \to W^+W^-H$

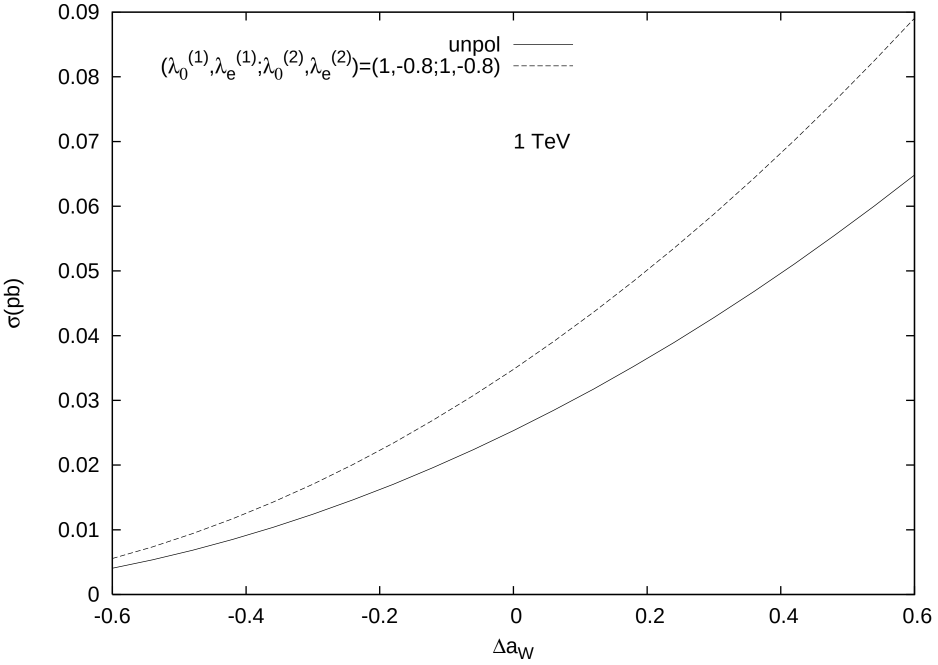

FIG. 3: The integrated total cross sections $\gamma\gamma \to W^+W^-H$ as a function of anomalous coupling Δa_W for $\sqrt{s} = 1TeV$. The legends are for initial beam polarizations.

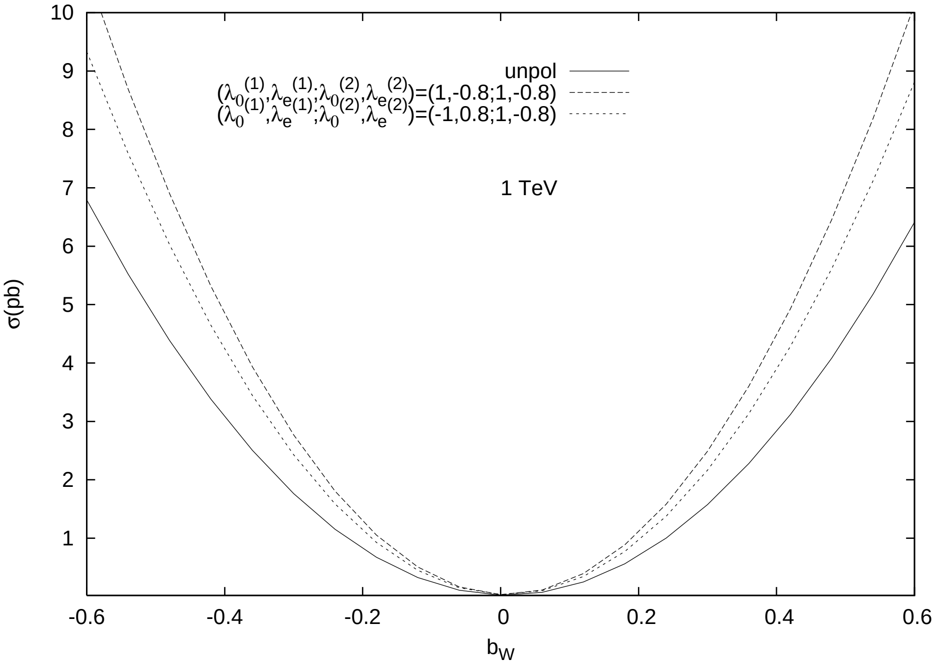

FIG. 4: The integrated total cross sections $\gamma\gamma \to W^+W^-H$ as a function of anomalous coupling b_W for $\sqrt{s} = 1TeV$. The legends are for initial beam polarizations.

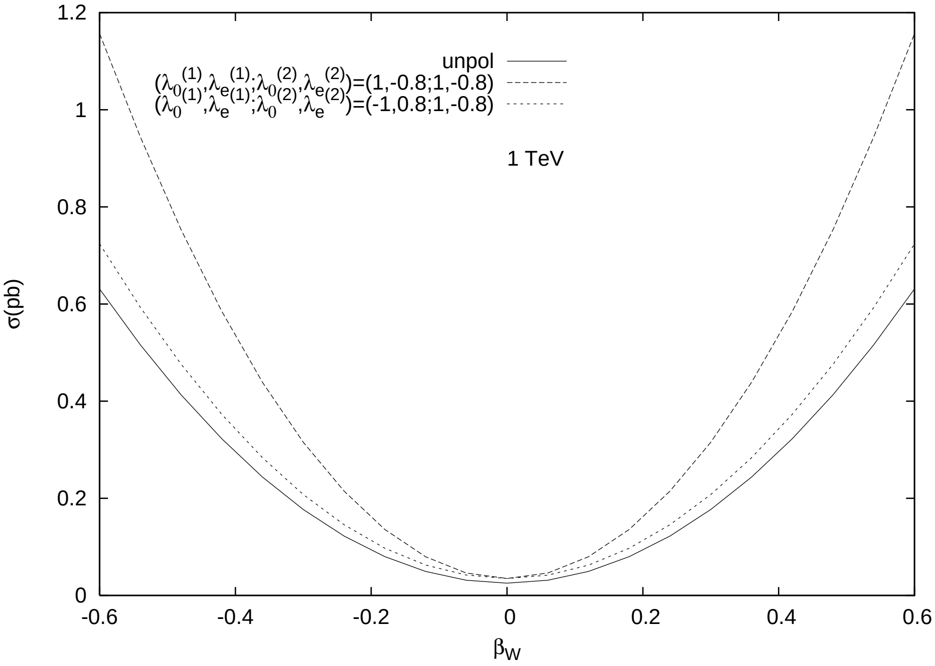

FIG. 5: The integrated total cross sections $\gamma\gamma \rightarrow W^+W^-H$ as a function of anomalous coupling β_W for $\sqrt{s} = 1TeV$. The legends are for initial beam polarizations.

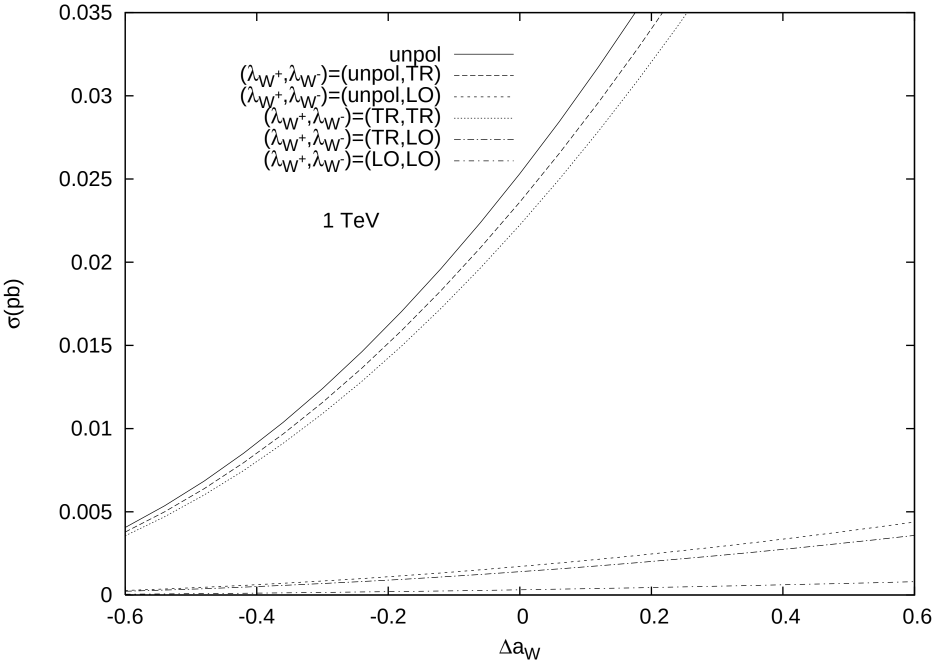

FIG. 6: The integrated total cross sections $\gamma\gamma \rightarrow W^+W^-H$ as a function of anomalous coupling Δa_W for $\sqrt{s} = 1TeV$. The legends are for final state polarizations.

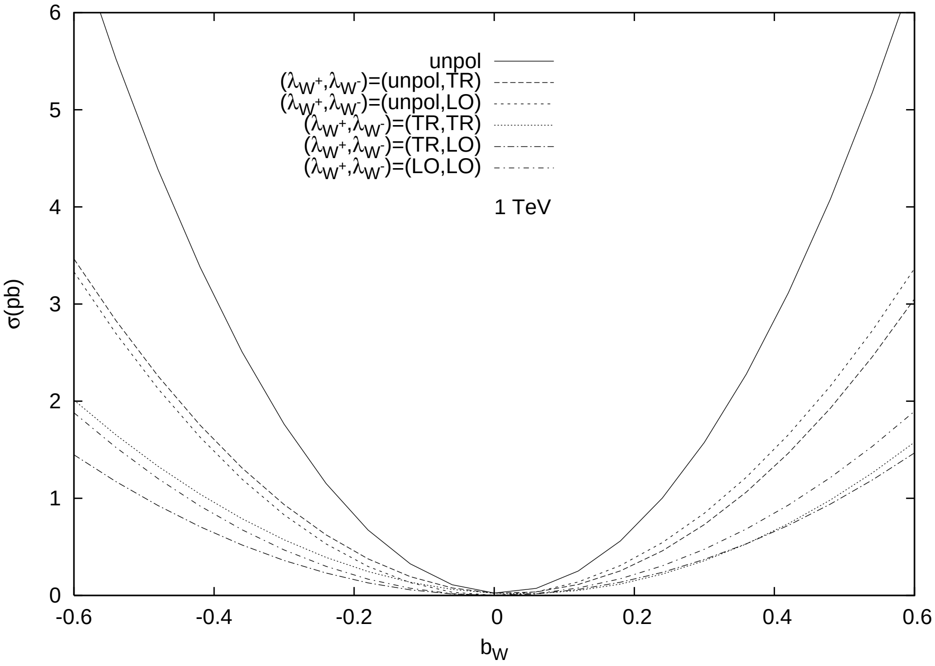

FIG. 7: The integrated total cross sections $\gamma\gamma \rightarrow W^+W^-H$ as a function of anomalous coupling b_W for $\sqrt{s} = 1TeV$. The legends are for final state polarizations.

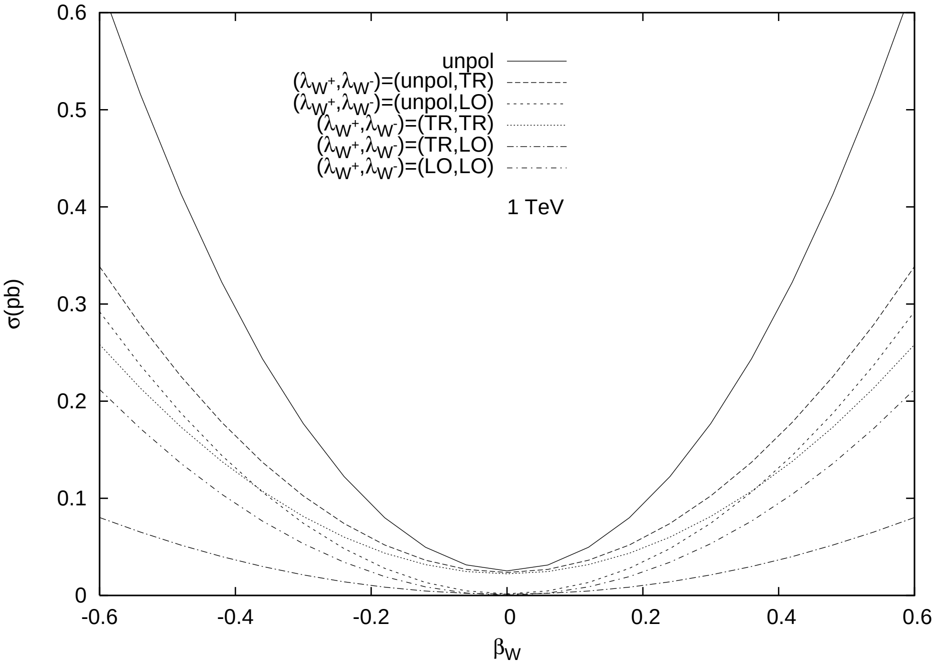

FIG. 8: The integrated total cross sections $\gamma\gamma \rightarrow W^+W^-H$ as a function of anomalous coupling β_W for $\sqrt{s} = 1TeV$. The legends are for final state polarizations.

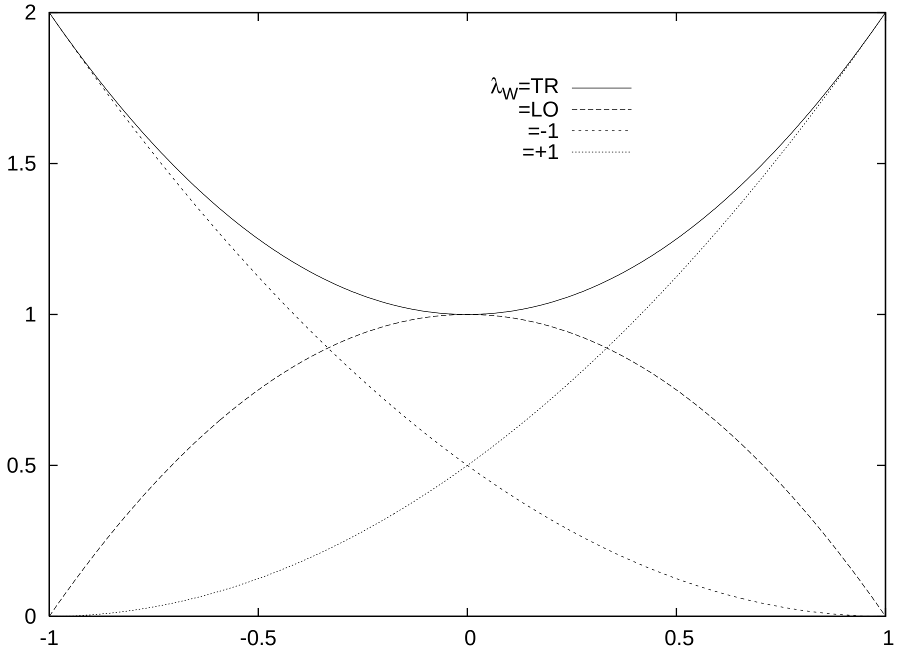

FIG. 9: $d^{\lambda_{W^-}}_{\lambda_{W^-}}$ versus $cos\theta$. The legends are for various polarization states of the final W^- boson.

TABLE I: Sensitivity of the $\gamma\gamma$ collision to anomalous WWH couplings at 95% C.L. for $\sqrt{s} = 1$ TeV and $L_{int} = 500$ fb^{-1}. The effects of initial beam polarizations and final state W^+, W^- polarizations are shown in each row. Only one of the couplings is assumed to deviate from the SM at a time.

$\lambda_0^{(1)}$	$\lambda_e^{(1)}$	$\lambda_0^{(2)}$	$\lambda_e^{(2)}$	λ_{W^+}	λ_{W^-}	Δa_W	b_W	β_W
0	0	0	0	TR+LO	TR+LO	(-0.0164, 0.0162)	(-0.0023, 0.0194)	(-0.0220, 0.0220)
0	0	0	0	TR	TR+LO	(-0.0170, 0.0167)	(-0.0022, 0.0398)	(-0.0300, 0.0300)
0	0	0	0	LO	TR+LO	(-0.0646, 0.0607)	(-0.0065, 0.0035)	(-0.0163, 0.0163)
0	0	0	0	TR	TR	(-0.0175, 0.0172)	(-0.0021, 0.0743)	(-0.0340, 0.0340)
0	0	0	0	TR	LO	(-0.0717, 0.0669)	(-0.0093, 0.0051)	(-0.0295, 0.0295)
0	0	0	0	LO	LO	(-0.1589, 0.1369)	(-0.0055, 0.0032)	(-0.0124, 0.0124)
+1	-0.8	+1	-0.8	TR+LO	TR+LO	(-0.0140, 0.0138)	(-0.0019, 0.0179)	(-0.0176, 0.0176)
-1	+0.8	+1	-0.8	TR+LO	TR+LO	(-0.0140, 0.0138)	(-0.0020, 0.0190)	(-0.0225, 0.0225)
+1	-0.8	+1	-0.8	TR	TR+LO	(-0.0144, 0.0142)	(-0.0019, 0.0399)	(-0.0270, 0.0270)
+1	-0.8	+1	-0.8	LO	TR+LO	(-0.0595, 0.0561)	(-0.0043, 0.0033)	(-0.0113, 0.0113)
-1	+0.8	+1	-0.8	TR	TR+LO	(-0.0144, 0.0142)	(-0.0019, 0.0384)	(-0.0282, 0.0282)
-1	+0.8	+1	-0.8	LO	TR+LO	(-0.0569, 0.0539)	(-0.0070, 0.0028)	(-0.0183, 0.0183)
+1	-0.8	+1	-0.8	TR	LO	(-0.0652, 0.0612)	(-0.0072, 0.0050)	(-0.0250, 0.0250)
-1	+0.8	+1	-0.8	TR	LO	(-0.0627, 0.0590)	(-0.0086, 0.0041)	(-0.0271, 0.0271)
+1	-0.8	+1	-0.8	TR	TR	(-0.0148, 0.0145)	(-0.0018, 0.0759)	(-0.0318, 0.0318)
+1	-0.8	+1	-0.8	LO	LO	(-0.1571, 0.1356)	(-0.0032, 0.0028)	(-0.0079, 0.0079)
-1	+0.8	+1	-0.8	TR	TR	(-0.0148, 0.0146)	(-0.0018, 0.0770)	(-0.0322, 0.0322)
-1	+0.8	+1	-0.8	LO	LO	(-0.1419, 0.1241)	(-0.0066, 0.0025)	(-0.0155, 0.0155)

TABLE II: The same as Table I but for $\sqrt{s} = 0.5$ TeV.

$\lambda_0^{(1)}$	$\lambda_e^{(1)}$	$\lambda_0^{(2)}$	$\lambda_e^{(2)}$	λ_{W^+}	λ_{W^-}	Δa_W	b_W	β_W
0	0	0	0	TR+LO	TR+LO	(-0.1239, 0.1102)	(-0.0207, 0.0161)	(-0.0725, 0.0725)
0	0	0	0	TR	TR+LO	(-0.1424, 0.1245)	(-0.0182, 0.0246)	(-0.0813, 0.0813)
0	0	0	0	LO	TR+LO	(-0.2844, 0.2198)	(-0.0373, 0.0122)	(-0.0912, 0.0912)
0	0	0	0	TR	TR	(-0.1605, 0.1381)	(-0.0159, 0.0370)	(-0.0888, 0.0888)
0	0	0	0	TR	LO	(-0.3635, 0.2629)	(-0.0411, 0.0153)	(-0.1082, 0.1082)
0	0	0	0	LO	LO	(-0.6145, 0.3607)	(-0.0397, 0.0159)	(-0.1067, 0.1067)
+1	-0.8	+1	-0.8	TR+LO	TR+LO	(-0.0870, 0.0801)	(-0.0099, 0.0262)	(-0.0590, 0.0590)
-1	+0.8	+1	-0.8	TR+LO	TR+LO	(-0.0863, 0.0794)	(-0.0261, 0.0089)	(-0.0630, 0.0630)
+1	-0.8	+1	-0.8	TR	TR+LO	(-0.0946, 0.0864)	(-0.0104, 0.0365)	(-0.0713, 0.0713)
+1	-0.8	+1	-0.8	LO	TR+LO	(-0.2482, 0.1978)	(-0.0168, 0.0161)	(-0.0606, 0.0606)
-1	+0.8	+1	-0.8	TR	TR+LO	(-0.1023, 0.0927)	(-0.0190, 0.0157)	(-0.0665, 0.0665)
-1	+0.8	+1	-0.8	LO	TR+LO	(-0.1726, 0.1469)	(-0.0512, 0.0070)	(-0.0946, 0.0946)
+1	-0.8	+1	-0.8	TR	LO	(-0.2869, 0.2213)	(-0.0230, 0.0199)	(-0.0875, 0.0875)
-1	+0.8	+1	-0.8	TR	LO	(-0.2247, 0.1828)	(-0.0487, 0.0089)	(-0.0924, 0.0924)
+1	-0.8	+1	-0.8	TR	TR	(-0.1020, 0.0925)	(-0.0103, 0.0492)	(-0.0790, 0.0790)
+1	-0.8	+1	-0.8	LO	LO	(-0.7443, 0.3909)	(-0.0152, 0.0172)	(-0.0545, 0.0545)
-1	+0.8	+1	-0.8	TR	TR	(-0.1181, 0.1056)	(-0.0136, 0.0289)	(-0.0717, 0.0717)
-1	+0.8	+1	-0.8	LO	LO	(-0.3029, 0.2305)	(-0.0624, 0.0098)	(-0.1749, 0.1749)